Heat Loss Quantification and Heat Transfer in Rotary Kilns for Calcination and Clinker Formation: From Combustion and Electrification at 150 kW to

Citation for the original published paper (version of record):
Qasim, I., Gunnarsson, A., Normann, F. et al (2025). Heat Loss Quantification and Heat Transfer in Rotary Kilns for Calcination and Clinker
Formation: From Combustion and Electrification at 150 kW to Industrial Scale. Industrial & Engineering Chemistry Research, 64(23): 11531-11543. http://dx.doi.org/10.1021/acs.iecr.5c00704

I&EC research
Industrial & Engineering Chemistry Research

pubs.acs.org/IECR
Article

Heat Loss Quantification and Heat Transfer in Rotary Kilns for Calcination and Clinker Formation: From Combustion and Electrification at 150 kW to Industrial Scale

Ibrahim Qasim,* Adrian Gunnarsson, Fredrik Normann, Bodil Wilhelmsson, Alexander Zether, and Klas Andersson

Cite This: https://doi.org/10.1021/acs.iecr.5c00704
Read Online

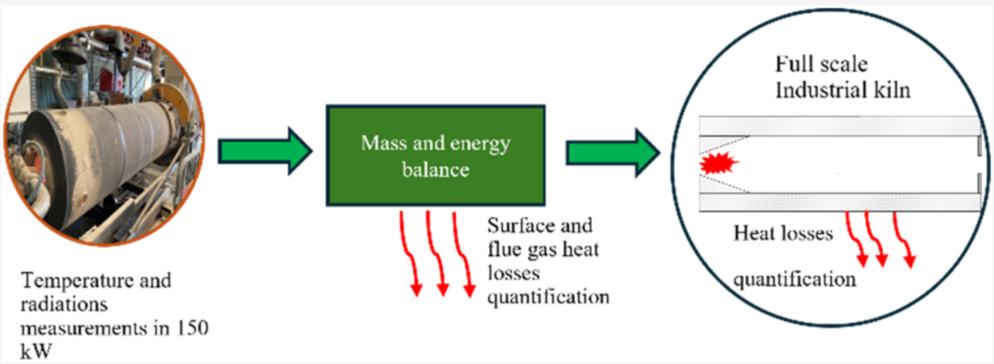

ABSTRACT: This study investigates heat transfer conditions and quantifies heat losses in a 150 kW rotary kiln with passing bed material. Measurements of gas and wall temperatures, gas compositions, and radiative heat transfer were conducted for propane combustion, oxygen-enriched propane, and resistance heating. Mass and energy balance results identify air leakage, flue gas losses, and surface heat losses as key heat loss mechanisms. For propane combustion, flue gas and surface losses accounted for 29 and 38% of total energy input, respectively. Oxygen-enriched propane reduced flue gas losses to 21%, while surface losses increased to 47% due to localized heat spots. Resistance heating provided uniform temperatures, with 52% surface losses and minimal 5% flue gas losses. Scaling analysis showed reduced surface losses at industrial scales—11% for propane, 12% for oxygen-enriched combustion, and 16% for electrification, while flue gas losses were 43, 19, and 5%, respectively. Energy transfer efficiency for calcination was quantified at 45% for propane and 60% for electrification. This work establishes a validated framework for measuring, quantifying, and scaling heat losses in rotary kilns.

1. INTRODUCTION

Cement is a fundamental material in construction, with global production exceeding four billion tons annually.[1] It is widely used in concrete production, providing durability and structural integrity. Cement production begins with quarrying limestone, which undergoes calcination at around 900 °C, releasing CO_2 and producing lime (CaO). This lime then reacts with other raw materials during clinkerization at temperatures up to 1450 °C to form key cement compounds such as alite and belite. For a detailed description of the cement production process, see, e.g., the work of Nielsen.[2]

The global target set by the United Nations is to limit the rise in average global temperature to below 1.5 °C.[3] To achieve this objective, the emission of greenhouse gases from the energy-intensive industrial sectors, such as the cement industry, needs to be significantly reduced. The cement industry alone is responsible for 8% of the world's greenhouse gas emissions.[4] Carbon dioxide emissions in cement production arise from two main sources: (i) process-related emissions and (ii) fuel-related emissions. The process emissions are mainly caused by the calcination reaction, notably limestone in the raw meal accounts for about 80% of the clinker raw material, resulting in the release of about 60% of the total cement production related CO_2 emissions.[5] The thermal energy required to calcinate the calcium carbonate and further ensure complete clinkerization, accounts for most of the fuel-related emissions and roughly the remaining 40% of the total CO_2 emissions for the cement process, primarily supplied by combustion of fossil fuels or alternative waste-derived fuels like car tires and plastics, selected

Received: February 21, 2025
Revised: May 22, 2025
Accepted: May 22, 2025

based on cost and availability.[6] Transitioning to low-carbon fuels is a key strategy for reducing emissions, but its impact is limited to fuel-related emissions, which account for about 40% of the total. It also alters heat transfer conditions, potentially affecting clinker quality.

Thermal behavior studies have long served as the foundation for understanding heat transport processes in industrial operations of cement kilns, including the contributions from conduction, convection, and radiation between gas, wall, and bed material, all essential to the kiln function, see e.g.,[7−10] However, a critical aspect of these studies involves conducting mass and energy balance analyses to quantify heat losses and improve kiln efficiency and a wide range of heat losses have been reported in the literature. Engin and Ari[11] conducted an energy audit analysis of a 50 m long dry-type rotary kiln system for cement production and concluded that radiation and convection losses from the surface of the kiln were 10.47% and 4.64% of total input, respectively. Further, they found that the total heat loss, including the hot flue gas and losses in the cooler stack amounted to 40% of the total input energy. Similar total heat loss estimations have been reported in previous studies. For example, Söğüt et al.[12] explored heat recovery in a rotary kiln used for a cement plant based on mass and energy balances, revealing that 5.1% of the input energy of the process was lost, caused by inefficiencies in the existing heat recovery mechanisms, again highlighting the importance of the overall design of the kiln system. Several studies addressing the energy balance in industrial-scale rotary kilns have been reported in the literature,.[13−17] These findings provide expected heat losses in industrial-scale rotary kilns and will be compared to our findings in an experimental cement rotary kiln and scale-up analysis.

While there are several means to reduce heat losses, it has been shown that air leakage is a major factor in rotary kilns, affecting process efficiency, energy consumption, and emission levels.[18] This has been displayed in a study by Acharya et al.[19] focusing on rotary kiln-based incinerators for hazardous waste treatment, showing that leakage air reduces the heat transfer rate to the solid bed. Others have created mathematical models to study the thermal and chemical behavior in the rotary kiln process, e.g., Shahin et al.[20] investigating three zones of a lime manufacturing process: the preheater, the rotary kiln, and the cooler, where they analyzed the effect of varying excess air levels on specific fuel consumption. By adjusting the secondary airflow to achieve different excess air percentages in their model while keeping the feed rate constant, they found that reducing excess air from 15 to 10% resulted in a 2.5% decrease in fuel use, highlighting the impact of air leakage on rotary kiln operations. Although these studies provide valuable insights into the effects of air leakage and excess air on rotary kiln performance, they did not use real process data to calculate the air leakage and focus on general principles without providing detailed derivation of the excess air coefficient. In this study, air leakage was quantified through mass balance calculations, forming the basis for energy balance estimations and the analysis of heat losses.

To better understand heat losses in rotary kilns, it is essential to examine heat transfer mechanisms and temperature profiles from both pilot- and industrial-scale systems. Tscheng and Watkinson[8] and Gorog et al.[21] conducted experiments to determine the convective heat transfer in pilot-scale rotary kilns, focusing on parameters such as rotational speed, gas flow rate, and fill ratio. While these studies provided valuable insights into gas-to-wall and gas-to-solids heat transfer, their validity for large-scale industrial kilns remains uncertain. In an internally heated rotary kiln, e.g., rotary kilns for cement production or iron ore pelletizing where heat is supplied from fuel combustion, the primary mode of heat transfer is through radiation.[22] Evaluating the performance of the cement process requires understanding and measuring the heat transfer conditions inside the kiln, particularly radiative heat transfer, which depends on the emissivity and temperature of the flame, wall, and bed. The gas emissivity is influenced by its composition, and entrained solids or dust from the bed can affect the overall emissivity and conductivity of the gas volume.[23] Radiative heat transfer in combustion systems has been extensively studied since the 1960s, with foundational models and theoretical approaches developed by Hottel and Sarofim,[24] Siegel and Howell,[25] and Modest[26] which continue to inform radiation modeling in current kiln studies. However, these models rely on simplifying assumptions and require experimental validation under realistic operating conditions. As such, experimental data sets particularly in complex, high-temperature environments like rotary kilns are still limited but crucial for validating and refining radiative heat transfer models for accurate application in industrial systems. In our previous work, we conducted radiative heat transfer measurements, which are scarce in literature, under various conditions in cylindrical furnaces[27−29] as well as within a 580 kW_{th} rotary kiln test furnace using coal and coal-biomass mixtures.[30] Temperature conditions of different laboratory or pilot-scale rotary kilns applying different heat sources have been measured by several researchers.[31−35] However, most of these temperature measurements primarily focus on the freeboard gas temperature. Also at a laboratory scale, a few studies have measured the temperature gradient within the bed inside the rotary kiln at a laboratory scale.[31,36] At an industrial scale, several studies have reported gas temperature profiles in rotary kilns for cement as well as spongy iron production.[23,37,38] In parallel to measurements, modeling work has been conducted to predict the thermal behavior of rotary kilns. Early efforts such as Spang[39] developed a dynamic model of cement kilns using partial differential equations, showing that the flame position and burning zone temperature can vary significantly during transient operation. Guruz and Bac[40] employed a zone-based approach for wet rotary kilns that explicitly includes radiative and convective heat losses from the kiln wall, allowing assessment of energy losses to the ambient environment. Singh and Ghoshdastidar[41] used CFD simulations in cement and alumina kilns to predict detailed temperature and heat flux distributions, highlighting the dominant role of radiative heat transfer in the burning zone, particularly due to gas radiation and entrained dust effects. However, detailed measurements of temperature and heat flux profiles for validation of such simulations is scarce in the literature. In this work, data sets of such data are presented, offering a basis for comparison and validation.

Given the need for rapid transformation of cement kilns to achieve net-zero emissions, understanding kiln heat transfer and heat losses is crucial to secure product quality and kiln performance. More so, understanding how these properties scale between demonstration and full-scale production units will be crucial for evaluating and developing new heating techniques. This work summarizes the heat transfer conditions of a series of experimental campaigns comparing combustion and direct electrification with the aim of quantifying kiln heat losses. Furthermore, the work will discuss how the conclusions from the demonstration scale will scale to full scale based on a heat and mass balance model.

https://doi.org/10.1021/acs.iecr.5c00704
Ind. Eng. Chem. Res. XXXX, XXX, XXX−XXX

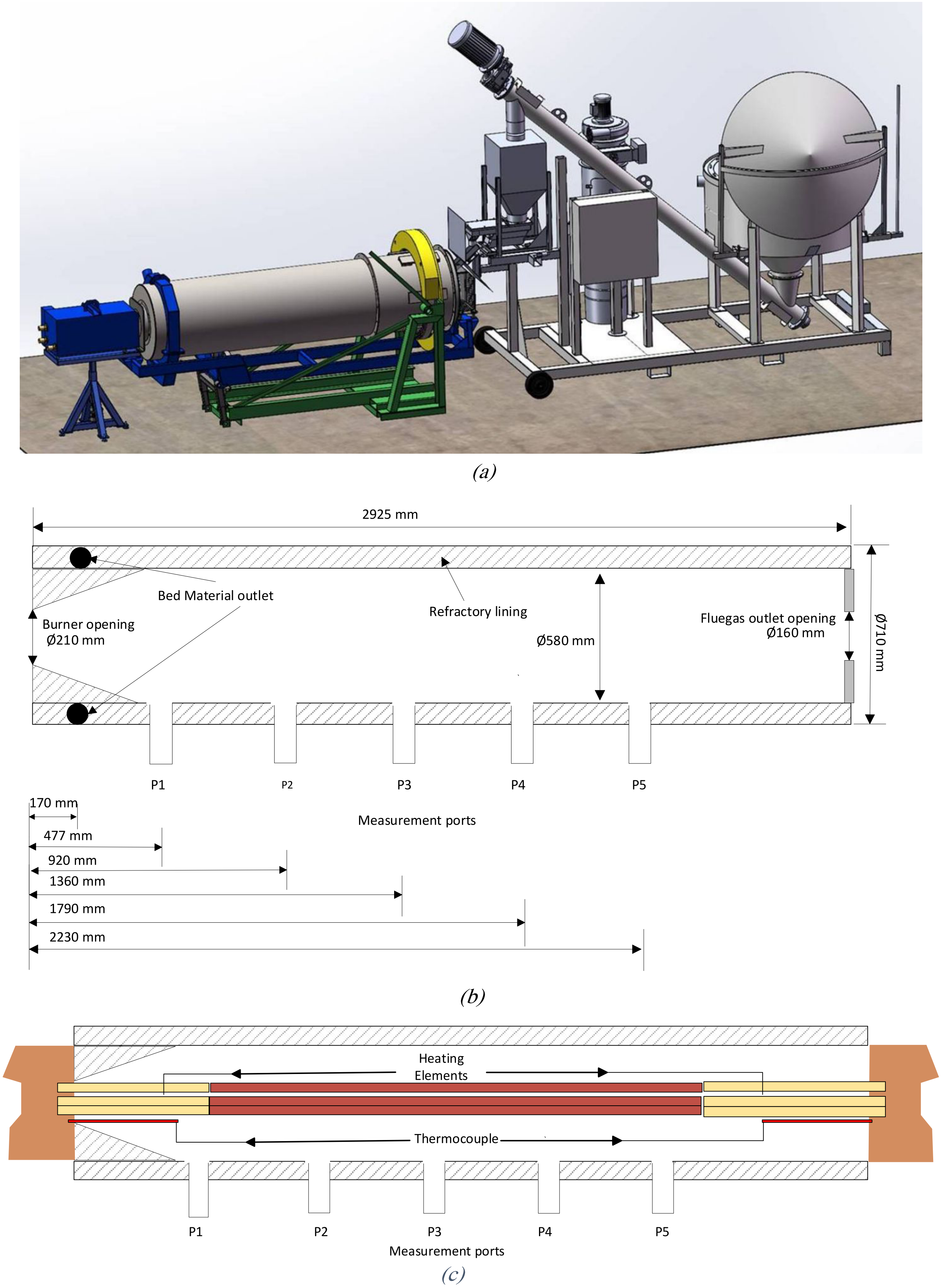

Figure 1. (a) 3-D model representation of Kiln Zero with the feeding system used during the experimental campaigns. (b) Dimensions of Kiln Zero operated with a propane burner. (c) Kiln Zero with resistance heating elements as a heat source.

https://doi.org/10.1021/acs.iecr.5c00704
Ind. Eng. Chem. Res. XXXX, XXX, XXX−XXX

2. METHODOLOGY

This study systematically evaluates heat transfer conditions in a scaled-down cement rotary kiln, focusing on key contributors to heat losses. The experimental methodology involved conducting measurement campaigns in a 150 kW rotary kiln system using three different heating technologies: propane combustion, oxygen-enriched combustion, and electrical resistance heating. Each test campaign was designed to measure wall and gas temperatures, gas composition, radiative intensity, and radiative heat flux under controlled conditions for several bed materials. These data sets were then used as input for mass and energy balance calculations to quantify heat losses and assess heat transfer conditions. The findings from the experiments also formed the foundation for subsequent scale-up analyses to evaluate energy efficiency and heat loss behavior at industrial scales.

2.1. Experiments. Two measurement campaigns were conducted in a 150 kW rotary kiln, referred to as Kiln Zero, to test various heat transfer technologies and raw bed materials for calcination and cement production. The experimental setup is illustrated in Figure 1a. Kiln Zero is cylindrical with a refractory wall, a steel shell, and is built to resemble a scaled-down version of an industrial cement rotary kiln and it is possible to adjust the inclination angle as well as the rotational speed of the kiln. To ensure a constant feed rate of raw material, a material feeder equipment was devised and installed at the kiln. The feeder system consists of a hopper and screw feeder that doses material into the higher end of the kiln. For certain materials, manual feeding was also possible when the automated feeding system was not suitable. Kiln Zero has an outer diameter of 0.71 m and an inner diameter of 0.58 m, with an overall length of 2.9 m. The steel shell layer has a thickness of 10 mm, complemented by a refractory lining of 55 mm. At the lower end of the kiln, the wall adopts a conical shape, and there are four evenly distributed openings where the bed material exits the kiln. At the higher end of the kiln, the bed material opening also acts as the flue gas outlet. To allow for measurements of the internal conditions of the kiln, five measurement ports, evenly distributed along the kiln axis are installed, numbered from P1, corresponding to the position close to the material outlet, to P5, corresponding to the position near the flue gas outlet. The dimensions of the experimental kiln and the port positions are depicted in Figure 1b. Kiln Zero may further be operated using various heating techniques. In this work, data is presented from operating the kiln with either a propane burner or resistance heating elements.

Operating Kiln Zero with a propane gas burner, the burner is positioned at the lower end of the kiln and consists of three registers, one for propane gas and one for axial and radial air, respectively. The propane gas flow, as well as the axial and radial air flows to the burner, were measured using Bronkhorst digital mass flow meters D-6360A-DF and D-6390-DF respectively. Additional oxygen can be introduced via the radial register to increase peak temperatures; however, the mass flow of oxygen was not measured. Additional air was introduced into Kiln Zero because of leaks at the burner, mainly caused by an open gap between the stationary burner and the rotating kiln.

Resistance heating elements powered by electricity were used as an alternative energy source. The heating elements, with a diameter of 55 mm and a length of 2.6 m, are precisely designed to fit the internal dimensions of the rotating drum, ensuring seamless integration into Kiln Zero. The heating elements have an effective emissivity of 0.88, which is a normal value for silicon carbide and is important in their performance. To match the design of Kiln Zero, which was intended for a maximum power of 150 kW, the heating components also provide a power output of 150 kW. The control of the heating elements within the kiln was executed in two distinct phases to ensure precision in temperature regulation. During the initial heating phase, the current was automatically regulated, with a predefined maximum amperage value serving as the only constraint. This approach facilitated a controlled ramp-up in temperature, minimizing the risk of thermal shock to the system. Upon reaching the desired operational temperature, the control strategy transitioned to manual intervention. Operators adjusted the power capacity manually. The inner gas temperature was continuously controlled by two installed thermocouples. In the present setup, three heating components were used. These elements are grouped in a staggered triangle arrangement, with each part separated by 75 mm.[32] The dimensions of the furnace remained unchanged from its prior application and a schematic of the placement of the resistance heating elements is shown in Figure 1c. A thorough analysis of the experimental setup, kiln design and operation can be found in the work by Jacob et al.,[32] employing both experiments and a steady-state 1-D model for analysis. The heating elements showed enhanced thermal efficiency in their study. However, concerns were raised about the short lifespan of silicon carbide heating elements and the risk of failure from dust accumulation.

Two heating technologies, i.e., propane gas and resistance heating elements, and four raw material mixtures were examined, two raw meals (RM) and two limestones (LS) as are presented in Table 1. It should be noted that the CO_2 and SO_3 values presented in Table 1 are derived from Loss on Ignition tests, representing the decomposition of carbonates (CO_2) and sulfates (SO_3) during heating via weight loss, and could potentially be recalculated into their respective carbonates. The raw meal refers to milled limestone with additives typical for cement production, while the limestone samples represent quarried and crushed stone used here to examine heat transfer behavior under varying thermal and material conditions. The particle size of RM was <100 μm and LS was 5−8 mm.

The experimental investigations were carried out in detail using propane gas as the reference case for bed materials RM1, RM2 (sets 1, 2, and 3), LS1 (sets 1 and 2), and LS2, where the sets indicate that the same bed material is tested but at different operation conditions. Electrified heating elements and propane combined with oxygen-enriched air were tested only for the LS2 bed material which was calcinated (clinker) for comparative analysis. The operational parameters are presented in Table 2.

Table 1. Chemical Composition of Bed Materials Used during Campaigns

		RM1	RM2	LS1	LS2
CaO	%	44.5	42.9	53.0	54.7
SiO_2	%	12.9	13.1	1.81	0.40
Al_2O_3	%	1.57	3.36	0.68	0.16
Fe_2O_3	%	3.07	1.89	0.32	0.06
MgO	%	1.19	2.85	1.20	0.47
K_2O	%	0.38	0.82	0.19	0.03
Na_2O	%	0.16	0.22	0.06	0.05
CO_2	%	37.0	34.6	44.3	45.7
SO_3	%	0.33	1.07	0.13	0.04

https://doi.org/10.1021/acs.iecr.5c00704
Ind. Eng. Chem. Res. XXXX, XXX, XXX−XXX

Table 2. Operational Conditions Used for Reference Propane Case, Oxygen-Enriched Case (Clinker), and Resistance Heating Element Case (Electrified)

Bed material	RM1	RM2 set 1	RM2 set 2	RM2 set 3	LS1 set 1	LS1 set 2	LS2	LS2 Clinker	LS2 Electrified
Bed feed [kg/h]	50	30	50	50	30	50	45	40	45
Propane feed [g/s] [kW]	2.3	2.4	2.19	2.17	2.84	2.7	2.87	3.32	
	106	111	102	100	132	125	134	154E	
Electrical input [kW]									140
Radial air feed [g/s]	6.3	6.1	5.2	5.2	11.6	5.7	12.8	11.2	
Axial air feed [g/s]	15.3	17.1	15.1	16.2	13.4	16.4	16.6	13.6	
Rotation [rpm]	3.3	3.3	3.7	2.7	4.0	2.7	2.7	3.8	

2.2. Measurements. During the campaign, wall temperature, gas composition, radiative intensity, and radiative heat flux were measured using probes inserted through five measurement ports (P1−P5) as shown in Figure 1b along the kiln axis. Measurements were taken by stopping kiln rotation momentarily, aligning the ports horizontally, and inserting the probes.

A narrow-angle radiometer (NAR) was used to measure radiative intensity along the probe's direct line of sight, by directing light rays toward a thermopile detector at the back end of the probe, calibrated using a blackbody furnace both before and after the measuring phase. Incident radiative heat flux on the kiln's inner wall was measured using a water-cooled ellipsoidal radiometer with a 2π sr viewing span, aligned with the inner wall at each port. The ellipsoidal radiometer and a similar NAR have been used in several previous studies, see.[42−44] An infrared (IR) camera (FLIR A655SC, 50 Hz, 640 × 120 pixels) measured surface temperatures of the inner and outer walls and the resistance heating elements. The IR camera could monitor temperatures up to 2000 °C and has also been used in previous studies.[30] Average wall temperatures were calculated using fixed emissivity (0.95). An emissivity value of 0.95 was selected based on the furnace's surface behavior and controlled conditions, which closely resembled a blackbody cavity. To ensure consistency across all tests, this value was used for all configurations, allowing direct comparison of relative changes due to heating technology, bed type, and process condition. Gas temperatures were measured with thermocouples (types B and K) at ports P2−P5 and at the flue gas outlet. All measurements were recorded after stabilization.

Gas samples from ports P2−P5 and the flue gas outlet were analyzed using a Fourier transform infrared (FTIR) spectrometer (MKS MultiGas 2030) and a HORIBA PG-250 analyzer. The FTIR, with a spectral resolution ranging from 0.5 to 128 cm^{-1} and a scan speed of up to 5 scans per second at 0.5 cm^{-1} resolution, measured H_2O, CO_2, and CO concentrations. The HORIBA PG-250 employed chemiluminescence for NOx detection, nondispersive infrared (NDIR) absorption for SO_2, CO, and CO_2, and a galvanic cell for O_2 measurement. It provided repeatability of ± 0.5% full scale (F.S.) for NOx (>100 ppm) and CO (>1000 ppm) and ±1.0% F.S. for other components, with a response time of approximately 45 s. Gases such as O_2, H_2O, CO_2, and CO were the primary focus, as these gases constitute the main portion of the flue gas stream, absorb and emit heat radiation, and are of interest due to emissions. For each measurement, a steady signal lasting roughly 2 min was sought.

The degree of calcination was determined from analyses of the mineral composition of the raw materials as well as the collected produced materials, using XRD. Crystal structures were established using Rietveld refinement and the mineralogy of the samples was analyzed with X-ray diffraction combined with the Rietveld method. Based on the amount of $CaCO_3$ in the raw material respectively in the product, the degree of calcination was readily determined from the fraction of the amount of mineral that had reacted and the amount of mineral in the raw material.

2.3. Measurement Uncertainty. Instrumental uncertainties were evaluated based on manufacturer specifications and applied calibration procedures. The FLIR A655sc IR camera has an accuracy of ±2 °C or ± 2% of reading, and the uncertainty is reflected in reported temperature error bars. Radiative intensity measurements using the Dexter 2 M thermopile-based NAR carry an estimated uncertainty of ±5%, based on NEP and calibration with a blackbody. Type B and K thermocouples used for gas temperatures have an accuracy of ±1.0 to ±1.5 °C. Gas composition measurements from the HORIBA and FTIR analyzer are accurate within ±2% of reading, following calibration with certified gas mixtures. Error bars are shown for all instruments in the result plots, while 95% confidence intervals were applied only to radiative intensity and flux data.

2.4. Mass Balance. The primary objectives of the mass balance analysis are to ensure control of the process, attain the excess air coefficient, the mass flow of leakage air, and the mass flow of flue gas. The mass flow gas balance was set up for the kiln as shown in eq 1.

$$\dot{m}_{\mathrm{fuel}} + \dot{m}_{\mathrm{air}} + \dot{m}_{\mathrm{CO_2,calc}} = \dot{m}_{\mathrm{fg}} \tag{1}$$

The mass flow of fuel input, $\dot{m}_{\mathrm{fuel}}$, was measured while the mass flow of carbon dioxide produced during the calcination reaction, $\dot{m}_{\mathrm{CO_2,calc}}$, is calculated from the molar flow feed of calcium carbonate in the bed material, $\dot{n}_{\mathrm{CaCO_3}}$, and the measured degree of calcination X_{calc}. The radial and axial air flows to the burner are measured, but the total mass flow of air, $\dot{m}_{\mathrm{air}}$, which is composed of the combustion air and the additional air entering due to leakage and the flue gas mass flow, $\dot{m}_{\mathrm{fluegas}}$, are unknown. Instead, the total airflow is calculated from the measured oxygen concentration $[O_2]$ at the kiln outlet. For the mass balance of the wet flue gas, it was assumed to consist of oxygen, nitrogen, carbon dioxide, and water, since the remainder of gases only result in small contributions in terms of mass. Based on the known oxygen concentration in the flue gas, the excess air coefficient (λ) can be derived as shown in eq 2. Detailed derivation of the excess air coefficient (λ) is given in the Supporting Information.

$$\lambda = \frac{5 + 2[O_2] + [O_2] \times \frac{X_{\mathrm{calc}} n_{\mathrm{CaCO_3}}}{n_{\mathrm{fuel}}}}{5\left(1 - \left([O_2] + [O_2] \times \frac{0.79}{0.21}\right)\right)} \tag{2}$$

For the clinkerization case with propane and oxygen-enriched air, the carbon dioxide from calcination reaction $\dot{m}_{\mathrm{CO_2,calc}}$ is

https://doi.org/10.1021/acs.iecr.5c00704
Ind. Eng. Chem. Res. XXXX, XXX, XXX−XXX

excluded (eq 1), since the bed feed consists of a fully calcinated meal, while the foundational assumption of flue gas consists of oxygen, nitrogen, carbon dioxide, and water remain unchanged. For the case with the resistance heating elements, a simplification was made, assuming that the flue gas only contained CO_2 produced from the calcination of bed material. This is justified by the fact that the kiln was closed from both ends and the occurring calcination reaction causes gases to leave the kiln, therefore the air leakage can be neglected in this case.

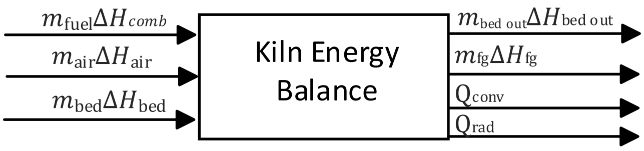

Figure 2. Energy Balance in the Kiln Zero System.

2.5. Energy Balance. An energy balance was set up to evaluate the heat losses (Q_{conv} + Q_{rad}), as is shown in Figure 2 and eq 3.

$$\dot{m}_{fuel}\Delta H_{comb} + \dot{m}_{air}\Delta H_{air} + \dot{m}_{bedin}\Delta H_{bedin} = \dot{m}_{bedout}\Delta H_{bedout} + \dot{m}_{fg}\Delta H_{fg} + Q_{conv} + Q_{rad} \quad (3)$$

Where $\dot{m}$ represents the mass flow, ΔH corresponds to enthalpy change, ΔH_{comb} is the heat of reaction from fuel combustion, ΔH_{bedout} represents the enthalpy of the bed material as it exits the kiln, and Q represent outer heat losses from the kiln outer surface due to convection and radiation. Subscripts *in* and *out* refers to any mass flows entering respectively leaving the kiln and *fg* refers to the flue gas. The air and bed material temperatures at the kiln's inlet were assumed to be at ambient levels (300 K) and, therefore, their energy contributions were considered negligible in the energy balance calculations.

The heat leaving the kiln with the bed material can be expressed from the heat of reaction for calcination and the heat capacities of the main component of the bed material, in accordance to eq 4.

$$\dot{m}_{bedout}\Delta H_{bedout} = \Delta H_{reac}X_{calc}\dot{m}_{bed,in} + \left(C_{pCaO}\frac{M_{CaO}}{M_{CaCO_3}}X_{calc} + C_{pCaCO_3}(1 - X_{calc})\right)(T_{bedout} - T_{ref})\dot{m}_{bed,raw} \quad (4)$$

The convective heat loss at the kiln shell is expressed in accordance with eq 5, using a correlation for a rotating cylinder from Barr et al.,[45] where *Re* corresponds to the Reynolds number, *Gr* represents the Grashof number, *Pr* represents the Prandtl number, *D* represents the outer diameter of kiln, *k* the thermal conductivity coefficient and *A* the shell area. The radiative heat loss was estimated using the net radiative heat exchange equation in accordance to eq 6 assuming an outer wall emissivity, ε, of 0.95 and an ambient temperature of 300 K.

$$Q_{conv} = \frac{k}{D}0.11\{(0.5Re^2 + Gr)Pr\}^{0.35}A(T_{outrshell} - T_{ref}) \quad (5)$$

$$Q_{rad} = \varepsilon\sigma A(T^4_{outershell} - T^4_{ambient}) \quad (6)$$

3. RESULTS AND DISCUSSION

Understanding the heat transfer conditions in rotary kilns requires detailed evaluation of temperature distributions, gas compositions, and radiative measurements. The temperature and gas composition results are input data to the mass and energy balance calculations. Radiative intensity and flux measurements are not applied in the mass and energy balance calculations, but they provide information about temperature and radiative conditions within the kiln and thereby assures the quality of the sampled data. The propane-fired reference conditions provide a baseline for evaluating heat transfer in the kiln.

3.1. Temperature. The inner and outer wall temperatures were measured for bed materials RM1, RM2 (sets 1−3), LS1 (sets 1−2), and LS2, see Tables 1 and 2. The results, shown in Figure 3, indicate a clear trend of decreasing inner wall temperature along the kiln axis, with maximum temperatures observed at ports 2 and 3. For RM cases, peak inner wall

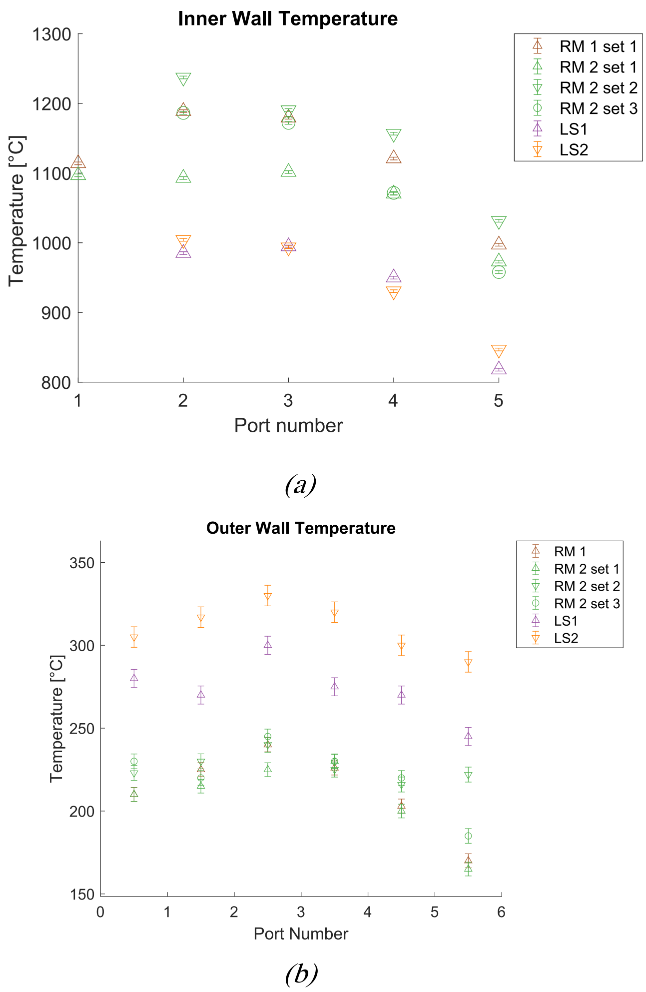

Figure 3. (a) Graph showing the distribution of inner wall temperature of reference calcination case with propane (b) Graph showing the distribution of outer wall temperature of reference calcination case with propane. Error bars shown in both inner and outer wall temperature plots represent the variations in the temperature observed during the measurement period at each respective port.

https://doi.org/10.1021/acs.iecr.5c00704
Ind. Eng. Chem. Res. XXXX, XXX, XXX−XXX

temperatures ranged from 1100 to 1250 °C, while LS cases exhibited lower peak values, approximately 1000 °C. Outer wall temperatures followed a similar decreasing trend, with maximum values observed between ports 2 and 3. RM cases exhibited lower outer wall temperatures (220−250 °C) compared to LS cases (270−330 °C), attributed to the insulating effect of the buildup coating layer in RM scenarios. The insulating properties of the buildup layer, observed only in RM cases, resulted in a larger temperature gradient between the inner and outer walls, emphasizing its significance in thermal efficiency. In contrast, LS materials displayed more uniform inner and outer wall temperatures, reflecting their different heat transfer characteristics.

3.2. Radiation. Radiative heat flux and intensity measurements are shown in Figures 4 and5, respectively. Heat flux values

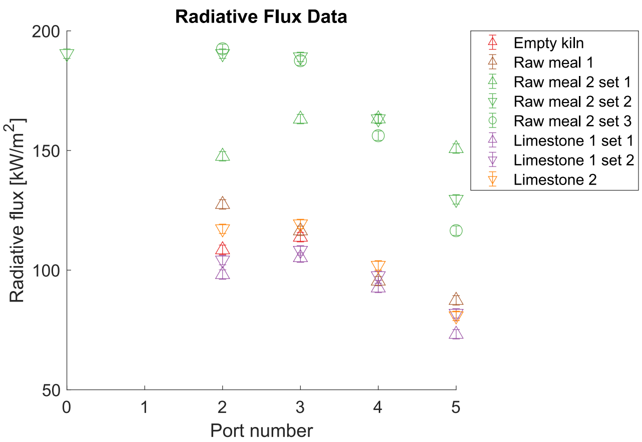

Figure 4. Radiative heat flux measurements collected through the measurement ports, using an ellipsoidal radiometer.

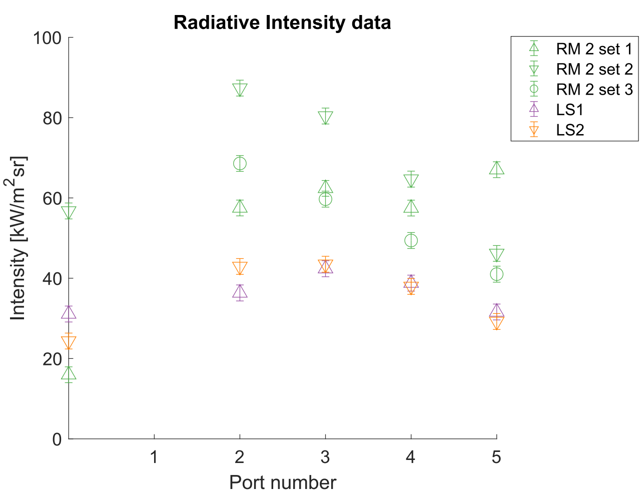

Figure 5. Radiative Intensity measurements collected in the different measurement ports, using a narrow angle radiometer.

primarily ranged between 100 and 200 kW/m^2, peaking at port 3. Additional measurements at port 0 (material outlet) showed lower fluxes, consistent with the reduced radiative impact at the outlet region. Measurements were also taken for the empty kiln, confirming baseline conditions for comparison with bed material experiments. Error bars in the figures represent signal fluctuations during the short measurement duration at each port. Radiative intensity trends mirrored those of heat flux, with peaks near port 3 and lower values near port 0. These measurements correlate strongly with inner wall temperature distributions, validating their significance in understanding localized radiative heat transfer. The radiation measurements validate the observed heat transfer conditions in the experimental-scale system.

3.3. Gas Composition. The gas concentrations of water and carbon dioxide were measured using an FTIR, while oxygen concentration was measured with a HORIBA system. Table 3

Table 3. Gas Composition Data for Test with Bed Material and Temperature of Flue Gas Measured at the Flue Gas Outlet

Bed material	H_2O [vol %]	O_2 [vol %]	CO_2 [vol %]	T [°C]
RM2-set 1	14	2.61	10.7	932
RM2-set 2	15.21	1.06	11.19	794
RM2-set 3	15.04	1.29	12.31	808
LS1-set 1	11.99	5.35	9.57	749
LS1-set 2	12.68	4.93	9.39	810
LS2	14.26	5.97	10.84	780

presents the gas composition data for bed material and temperature of flue gas measured with thermocouples at the flue gas outlet used in the mass and energy balance analysis. Detailed gas composition data for each measurement port can be found in Figures S1−S3 in Supporting Information.

3.4. Mass and Energy Balances. Table 4 presents the cases in which the required data to close the mass balance were available and the calculated excess of air and air leakage. The mass flow rate of propane fuel, m_{fuel}, feeding rate of bed material, m_{bed}, and the degree of calcination, X_{calc}, presented in Table 4 were all measured during experiments. The air leakage presented in the table refers to the percentage of the total airflow entering the system that is due to leakage. According to the findings, the calcination process using propane gas is characterized by significant air leakages followed by high mass flow rates of flue gas. In comparison, the clinkerization process, which uses a mixture of propane gas and oxygen-enriched air, has lower air leakage, due to the increased pressure at the kiln's fuel entrance point as a result of the increased flow of propane and the additional flow of pure oxygen, followed by a calculated lowered mass flow rate of flue gas. In the resistance heating case, the flue gas flow is minimal, consisting only of CO_2 generated by the calcination reaction.

The energy balance analysis is summarized in Table 5, where Q_{in} represents heat input from fuel combustion, and Q_{out} includes heat transferred via flue gas, bed material, and radiative and convective losses. The "Error %" indicates the percentage difference between the left and right sides of the energy balance equation (eq 3). These calculations incorporate mass balance data and additional temperature measurements of the flue gas and kiln's outer wall, as detailed in the methodology.

For propane combustion with oxygen-enriched air, a flue gas temperature of 1100 °C was assumed based on IR measurements and empirical data. Similarly, for resistance heating, a flue gas temperature of 900 °C was used. The input energy for resistance heating, calculated from electrical current and voltage, was 140 kW. The heating elements exhibited the highest radiative and convective heat losses at the kiln's outer wall, accounting for 52% of the total energy input. These results are consistent with Jacob et al.,[32] who reported 55% heat losses in a similar electrically heated rotary kiln. Comparatively, outer wall heat losses for propane with oxygen-enriched air were slightly lower, at 47% of the total input energy. These findings

https://doi.org/10.1021/acs.iecr.5c00704
Ind. Eng. Chem. Res. XXXX, XXX, XXX−XXX

Table 4. Calculated and Measured Mass Flows

Fuel source	Bed material	m_{fuel} [kg/h]	m_{bed} [kg/h]	X_{calc} [%]	m_{fg} [kg/h]	λ	Air leakage [%]
Propane gas	RM2-set 2	7.74	50	99	158.4	1.06	38
Propane gas	RM2-set 3	7.77	50	99	169.2	1.16	48
Propane gas	LS1−set 1	10.11	30	90	244.8	1.43	65
Propane gas	LS1−set 2	10	50	99	221.0	1.31	61
Propane gas	LS2	10.2	50	99	223.2	1.2	59
Propane + O_2	LS2 Clinker	11.95	40	99	104.4	1.06	2.7
Heating elements	LS2 Electrified		60	99	25.92		

Table 5. Energy Balance Results

Heating source	Bed material	m_{fuel} [kg/h]	m_{bed} [kg/h]	Q_{conv} [kW]	Q_{rad} [kW]	Q_{in} [kW]	Q_{out} [kW]	Error %
propane	RM2-set 2	7.74	50	10.1	19.2	99.7	98.1	**2**
propane	RM2-set 3	7.77	50	8.9	14.9	100.2	92.7	**8**
propane	LS1−set 1	10.11	30	16.7	48	132	128	**4**
propane	LS1−set 2	10.04	50	15.4	38.4	130	125	**4**
propane	LS2	10.29	50	13.7	31	132	124	**6**
propane + pure O_2	LS2−Clinker	11.95	40	17	55.5	154	137	**12**
heating elements	LS2-Electrified		60	18.3	54.9	140	117	**18**

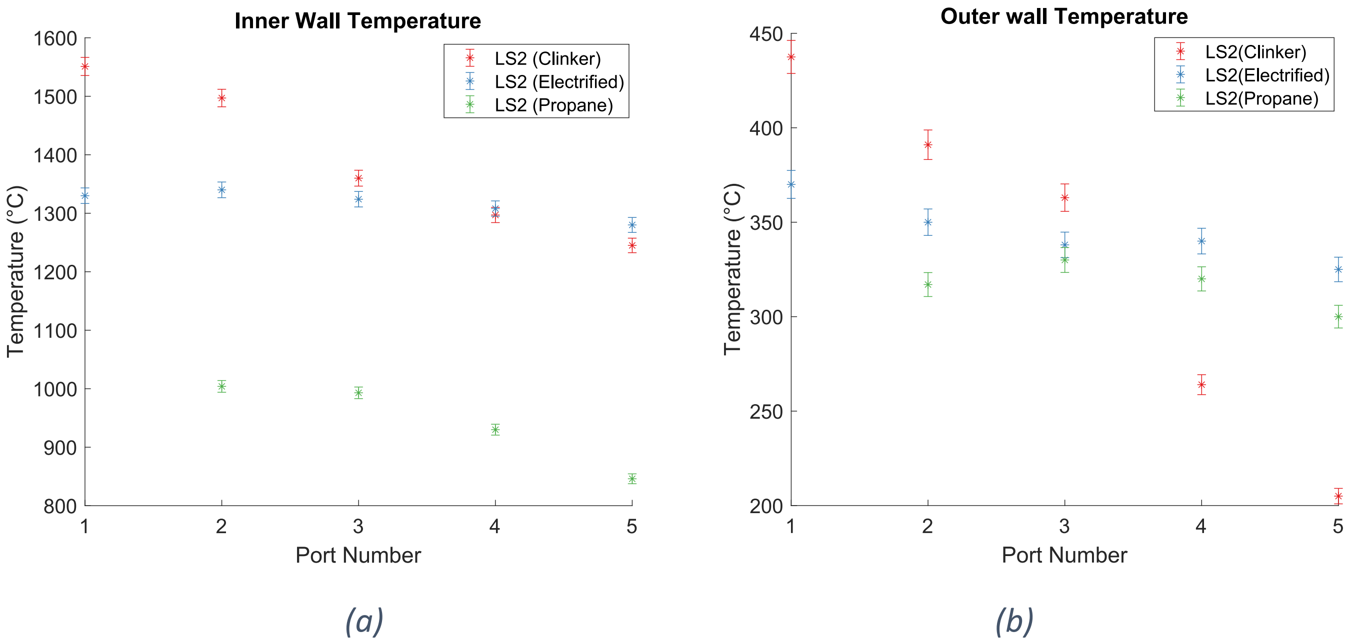

Figure 6. Comparison of (a) inner and (b) outer wall temperature measured by IR camera for LS2 (propane), LS2 (clinker), and LS2 (electrified). The error bars represent the variation in temperature during the measurement period at respective ports.

demonstrate the significant influence of heating methods on heat loss mechanisms and energy efficiency.

The error percentages for the energy balances were <15% in all cases, except for the resistance heating scenario, reflecting the overall reliability of the results. The sensitivity analysis highlighted the importance of outer wall and flue gas temperatures as both directly influenced radiative and convective heat losses.

3.5. Comparison of Heating Technologies. This section examines the thermal performance using resistance heating elements, oxygen-enriched combustion and conventional combustion conditions using bed material LS. Operating parameters are detailed in Table 2.

Conventional combustion conditions (reference case) and oxygen-enriched combustion showed nonuniform temperature profiles (Figure 6a) as compared to the resistance heating. However, conventional combustion showed higher convective losses through the flue gas due to greater air leakage and higher flue gas volumes as compared to oxygen-enriched combustion (29% in propane combustion vs 21% in oxygen-enriched combustion). The reduction in flue gas losses for the oxygen-enriched case can be attributed to the lower air-to-fuel ratio, which decreases the overall flue gas volume. The improved combustion efficiency and higher flame temperatures enhance heat transfer to the bed material and inner walls, reducing the proportion of energy carried away by the flue gas. The higher inner wall temperatures reaching up to ∼1550 °C at port 1 in the oxygen-enriched setup (Figure 6a) indicate enhanced heat transfer to the bed material. However, localized surface losses near the burner were observed, emphasizing the trade-offs associated with this technology. The experimental results align with theoretical expectations, where reduced flue gas flow

https://doi.org/10.1021/acs.iecr.5c00704
Ind. Eng. Chem. Res. XXXX, XXX, XXX−XXX

minimizes convective heat losses and improves energy retention within the kiln. These findings highlight the potential for oxygen-enriched combustion to improve energy utilization in rotary kilns. Wall temperature and gas temperature profiles inside the kiln for different fuels similar to Figure 6a have been reported in rotary kiln studies.[17,31,35,45]

Resistance heating demonstrated a uniform temperature distribution along the kiln axis, particularly between ports 2 to 4, minimizing thermal gradients and providing stable heating conditions ideal for calcination (Figure 6a). Jacob et al.[32] presented their modeling work using resistance heating elements showing a peak temperature of 980 °C inside a rotary kiln heated with electrical heating elements. However, unlike the present study, the inner wall temperature was not uniform along the kiln axis in their modeling results. The absence of flue gas convective losses shifted the energy loss profile, with surface radiative and convective losses accounting for approximately 52% of the total input energy. The absence of a combustion process in the electrification case significantly reduced flue gas generation, resulting in only 5% of the total energy losses attributed to flue gas heat losses. While uniform heating reduces the risk of localized overheating and underheating, improving process stability, it leads to increased surface heat losses due to prolonged exposure of the kiln shell to elevated temperatures.

The results of the comparative analysis of radiative intensity measured from inner wall of the kiln are shown in Figure 7. For

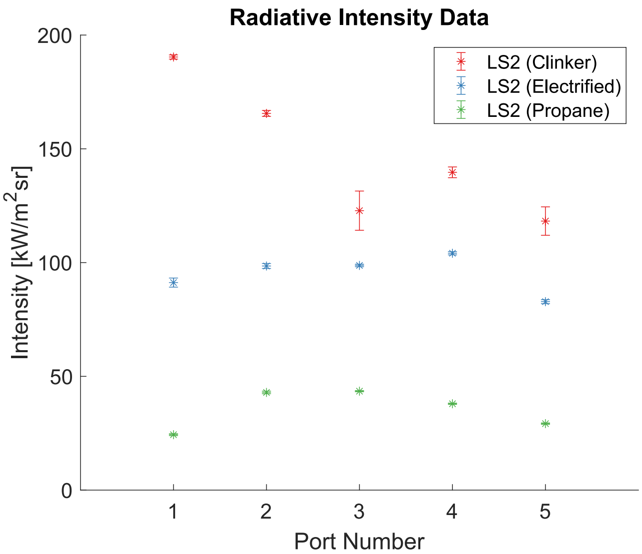

Figure 7. Comparison of radiation intensity measured by NAR for LS2 (propane), LS2 (clinker), and LS2 (electrified). The error bars represent the variation in intensity signal during the measurement period at respective ports.

resistance heating, intensity peaked between ports 2 and 4, correlating with the calcination zone. Oxygen-enriched propane exhibited its maximum radiative intensity at port 1, emphasizing the significant radiative contribution in the initial flame zone. These measurements provide supplementary validation for the observed inner wall temperature profiles.

3.6. Scaling Results. The scaling analysis evaluates how heat transfer conditions and energy efficiency change when transitioning from the 150 kW scale experiments in Kiln Zero to industrial-scale rotary kilns. By applying heat loss methodologies and parameters from the smaller scale to larger systems, the aim is to assess the feasibility of scaling advanced heating technologies such as oxygen-enriched propane combustion and resistance heating, and to compare the findings with industrial scale kilns.

Table 6 compares flue gas heat loss (Q_{fg}) and surface heat losses (Q_{losses}) from the outer kiln shell across industrial kilns

Table 6. Comparison of Outer Shell Surface Heat Losses and Flue Gas Losses from Energy Balance in Industrial-Scale Rotary Kilns and the Present Experimental Rotary Kiln[a]

Authors	Q_{fg} [%]	Q_{losses} [%]	Scale of rotary kiln
Engin and Ari[11]	19	15	D = 3.6 m, L = 50 m
Ustaoglu et al.[17]	33	54	D = 3.4 m, L = 120 m
Utlu et al.[14]	27.1	15	82.9 ton-clinker/h
Söğüt[12]		5.1	39.50 ton-clinker/h
Atmaca and Yumrutas[13]	32.6	11.2	D = 4.2 m, L = 59 m
Nasution et al.[15]	12.3	30.7	D = 5.6 m, L = 84 m
Boateng[16]	33.3	13.5	D = 3.35 m, L = 92 m
Present study RM2−set 2	38	29	D = 0.77 m, L = 2.9 m
Present study LS2-Clinker	21	47	D = 0.77 m, L = 2.9 m
Present study LS2-Electrified	5	51	D = 0.77 m, L = 2.9 m

[a]The kiln scales are listed based on their diameters (D) and lengths (L) or production capacity

using conventional heating methods and Kiln Zero under various conditions. The data reveal significant differences: industrial kilns generally show reduced surface heat losses due to optimized designs and lower surface-to-volume (S/V) ratios. For example, Atmaca and Yumrutas[13] achieved low heat losses through improved refractory materials, while Söğüt et al.[12] demonstrated even further reductions by incorporating heat recovery exchangers. In contrast, Kiln Zero exhibited higher heat losses—29% for propane combustion, 47% for oxygen-enriched propane, and 51% for resistance heating—primarily due to its experimental design and smaller S/V ratio. Nevertheless, the present study's heat losses are still comparable to Nasution et al.[15] and Ustaoglu et al.[17] These comparisons validate the methodology while illustrating the impact of kiln design and scale on heat transfer conditions.

The energy balance was extended to industrial-scale kilns under similar conditions to Kiln Zero to assess how heat losses evolve with scale. Parameters from Boateng's study (dimensions 3.35 m diameter, 92 m length)[16] of 62.4 MW, which focused on calcination, and the HMC kiln (dimensions 5.6 m diameter, 80 m length) of 116 MW, designed for clinkerization, were employed to represent two distinct modes of industrial operation. Scaling parameters, presented in Table 7, include L/D ratio, S/V ratio, and bed material residence time calculated using the established equation by Sullivan et al.,[46] and gas velocity calculated based on volumetric flow and considering the

Table 7. Comparison of Scaling Parameters of the Kiln Zero, Boateng Study, and an Industrial Kiln of HMC

	L/D	S/V	Bed material residence time (mins)	Heat supply per kg (kJ/kg)	Gas velocity (m/s)
KilnZero (scale down)	4.1	5.6	8.8	9496.4	0.66
Boateng kiln[16]	20.5	0.8	48.4	4781.6	10.1
HMC kiln	14.3	0.71	25.1	1094.3	3.4

https://doi.org/10.1021/acs.iecr.5c00704
Ind. Eng. Chem. Res. XXXX, XXX, XXX−XXX

Table 8. Heat and Flue Gas Losses for Different Heat Transfer Technologies from the Present Scale-Up Study Compared with Boateng's Study and Heidelberg Materials Cement (HMC) Data[a]

	Propane		Oxygen-enriched case		Electrical resistance heating	
	Q_{fg} (%)	Q_{losses} (%)	Q_{fg} (%)	Q_{losses} (%)	Q_{fg} (%)	Q_{losses} (%)
Present study	38	29	21	47	5	52
Present study scale up	43	11	18.5	12	12	20
Boateng[16]	39	13.3				
HMC kiln			27	10.6		

[a]The percentages represent the heat losses as a fraction of the total input energy.

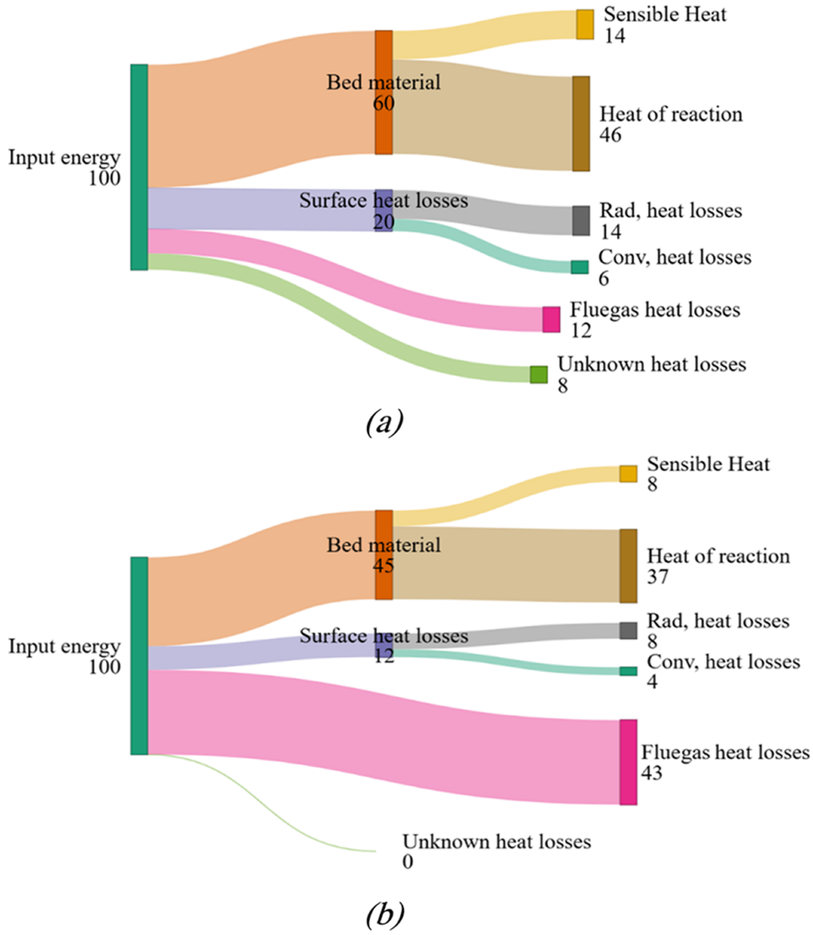

Figure 8. Sankey diagrams representing the energy balance for the calcination process using (a) electrification and (b) conventional combustion. The numbers represent the percentages of total energy input.

inner diameter of the kilns. Assumptions from Kiln Zero, such as emissivity (0.95) and outer wall temperature profiles, were retained to maintain consistency. To maintain the same energy supply as in the study by Boateng for the calcination process, the propane and bed material feed rates were adjusted to match the energy input of 62.4 MW. The calculated air-to-fuel ratio is kept the same as Kiln Zero, meaning that the flue gas composition is the same at the gas outlet.

The results of the scaled-up energy balance are summarized in Table 8. The scaled-up results for the propane-fired kiln for calcination are compared with Boateng's kiln, while the oxygen-enriched propane case for clinker formation is compared with the HMC kiln, using their respective dimensions. It is important to note that the HMC kiln is not operated in an oxygen-enriched atmosphere, unlike Kiln Zero, which assumes oxygen enrichment in its scaled-up analysis. This approach provides a direct comparison of heat loss mechanisms and energy distributions between the demonstration and industrial scales.

The Sankey diagrams in Figure 8 show energy distribution, detailing the heat transfer mechanisms for both combustion and electrification technologies. These diagrams highlight energy transfer efficiency, defined as the percentage of total energy input transferred to the bed material. For propane combustion, energy transfer to the bed material accounted for 45% of total input energy and flue gas losses (Q_{fg}) increased slightly to 43% in the scaled system due to higher gas velocities and feed rates. The increase in gas velocity, calculated based on volumetric flow and kiln diameter, reflects the larger scale and higher feed throughput in industrial kilns. This higher flow rate increases convective heat losses via the flue gases. In contrast, surface heat losses (Q_{losses}) decreased significantly to 11%, due to the reduced surface-to-volume S/V ratio of the scaled kiln. In the oxygen-

https://doi.org/10.1021/acs.iecr.5c00704
Ind. Eng. Chem. Res. XXXX, XXX, XXX−XXX

enriched propane combustion case applied to the HMC kiln, flue gas losses decreased to 18.5% compared to the experimental scale results. This reduction can be due to the reduced air-to-fuel ratio and increased combustion efficiency, leading to lower flue gas volumes and temperatures. However, surface heat losses remained comparable, particularly near the burner and central zones of the kiln, where higher flame temperatures resulted in increased radiative losses. The HMC kiln, operated under conventional propane combustion without oxygen addition, showed higher flue gas losses (27%) in comparison, highlighting the potential benefits of oxygen-enriched systems for improving energy utilization.

These results underscore the complex interplay between flue gas and surface heat losses during scaling. While flue gas losses are more sensitive to gas velocity and feed rate, surface losses depend heavily on the kiln's geometry and thermal properties. The findings highlight the importance of optimizing heating technologies and operational parameters during scaling to achieve a balance between minimizing convective and radiative losses while maximizing energy transfer to the bed material.

Scaling comparisons are more challenging for resistance heating due to the absence of large-scale operational data. The analysis revealed a reduction in surface heat losses from 52% in the experimental kiln to 20% at the industrial scale. This trend aligns with combustion processes, where the surface-to-volume ratio decreases with scaling, lowering surface heat losses proportionally. However, the scaled-up surface heat losses for resistance heating remained higher than those for propane (11%) and oxygen-enriched combustion (12%), likely due to the uniform temperature distribution characteristic of resistance heating. Unlike nonuniform profiles in combustion, which show localized heat loss variations, uniform heating results in consistently elevated surface temperatures along the kiln, increasing overall surface heat losses. Flue gas heat losses in the resistance heating case were notably low at 12% in the scaled system compared to propane and oxygen-enriched propane. This reduction reflects the absence of air leakage and combustion, with flue gas composed solely of CO_2 generated from the bed material. The higher feed rate at the industrial scale increased CO_2 generation, explaining the rise from 5% in the experimental kiln to 12% at the industrial scale. The efficiency of the electrification process for calcination was estimated to be 60% higher than that of conventional propane combustion.

This study shows how advanced heating technologies could complement existing designs by combining demonstration scale data with industrial-scale parameters. The comparison of scaled-up energy balance results with literature data validates the methodology and highlights differences between demonstration and industrial systems. The study underlines the importance of understanding heat losses as a critical parameter for scaling rotary kilns from experimental to industrial systems.

4. CONCLUSIONS

This work presents a comprehensive evaluation of heat loss terms and their scalability in cement rotary kilns using three different heating technologies: combustion, oxygen-enriched combustion, and electrification by resistance heating. Detailed measurements of gas and wall temperatures, gas composition, radiative intensity, and heat flux were used to analyze heat transfer conditions. The study quantifies heat losses through mass and energy balances, emphasizing critical parameters such as air leakage, fuel flow rates, and outer shell temperature control.

The work concludes with

- A critical role of air leakage for thermal efficiency, which favors electrical heating and oxygen-enriched propane combustion over propane combustion.
- Oxygen-enriched propane combustion reduced flue gas flow rates and thereby reduced heat losses with the outlet flue gas stream, improving overall energy efficiency compared to conventional propane combustion.
- Oxygen addition to combustion processes notably improved kiln efficiency and heat transfer, as evidenced by higher inner wall temperatures and radiative intensities.
- Temperature and radiative intensity measurements showed that electrically powered resistance heating elements provided stable heat conditions, ensuring consistent heat transfer crucial for effective calcination.
- In the full-scale kiln analysis, the decrease in surface-to-volume ratio and higher feed rates resulted in a significant reduction in surface heat losses from 29 to 11% in the propane case, from 47 to 12% in the oxygen-enriched propane case, and from 52 to 16% in resistance heating element case highlighting the importance of scale when considering heat transfer conditions.
- Scale-up analysis highlights that flue gas losses are sensitive to gas velocity and feed rate while surface heat losses depend on kiln geometry and thermal properties of the kiln wall.
- Energy distribution analysis in scale-up showed that energy transfer to the bed material increased from 45% in conventional propane combustion to 60% in electrification.

■ ASSOCIATED CONTENT

Supporting Information

The Supporting Information is available free of charge at https://pubs.acs.org/doi/10.1021/acs.iecr.5c00704.

Derivation of excess air coefficient, including combustion equations and oxygen balance, and additional gas composition measurements (H_2O, CO_2, O_2) with instrument accuracy and error bars (PDF)

■ AUTHOR INFORMATION

Corresponding Author

Ibrahim Qasim − *Department of Space, Earth and Environment, Chalmers University of Technology, SE-412 96 Gothenburg, Sweden*; orcid.org/0009-0002-2832-849X; Email: ibrahim.qasim@chalmers.se

Authors

Adrian Gunnarsson − *Department of Space, Earth and Environment, Chalmers University of Technology, SE-412 96 Gothenburg, Sweden*; orcid.org/0000-0003-0352-948X

Fredrik Normann − *Department of Space, Earth and Environment, Chalmers University of Technology, SE-412 96 Gothenburg, Sweden*

Bodil Wilhelmsson − *Heidelberg Materials Cement Sverige AB, SE-100 74 Stockholm, Sweden; Department of Applied Physics and Electronics, Umeå University, SE-901 87 Umeå, Sweden*; orcid.org/0000-0001-8527-7145

Alexander Zether − *Heidelberg Materials Cement Sverige AB, SE-100 74 Stockholm, Sweden*

https://doi.org/10.1021/acs.iecr.5c00704
Ind. Eng. Chem. Res. XXXX, XXX, XXX−XXX

Klas Andersson − *Department of Space, Earth and Environment, Chalmers University of Technology, SE-412 96 Gothenburg, Sweden;* orcid.org/0000-0001-5968-9082

Complete contact information is available at:
https://pubs.acs.org/10.1021/acs.iecr.5c00704

Notes

The authors declare no competing financial interest.

■ ACKNOWLEDGMENTS

This work was conducted within the CemZero project, funded by the Swedish Energy Agency under project number P2021-00015.

■ REFERENCES

(1) U.S. Geological Survey. *Cement Statistics and Information* U.S. Geological Survey: Reston, VA, 2023.
(2) Nielsen, A. R. Combustion of Large Solid Fuels in Cement Rotary Kilns. Ph.D. Thesis, Technical University of Denmark: Lyngby, Denmark, 2012.
(3) UNFCCC. *Adoption of the Paris Agreement*; United Nations Office: Geneva, Switzerland.
(4) Wilhelmsson, B.; Kollberg, C.; Larsson, J.; Eriksson, J.; Eriksson, M. *CemZero − A Feasibility Study Evaluating Ways to Reach Sustainable Cement Production via the Use of Electricity*; Vattenfall AB and Cementa AB: Stockholm, Sweden, 2018.
(5) Carriço, A.; Bogas, J. A.; Guedes, M. Thermoactivated Cementitious Materials − A Review. *Constr. Build. Mater.* **2020**, *250*, No. 118873.
(6) Zieri, W.; Ismail, I. Alternative Fuels from Waste Products in Cement Industry. In *Handbook of Ecomaterials*; Springer International Publishing: Cham, 2019; pp 1183−1206.
(7) Watkinson, A. P.; Brimacombe, J. K. Heat Transfer in a Direct-Fired Rotary Kiln: II. Heat Flow Results and Their Interpretation. *Metall. Trans. B* **1978**, *9* (2), 209−219.
(8) Tscheng, S. H.; Watkinson, A. P. Convective Heat Transfer in a Rotary Kiln. *Can. J. Chem. Eng.* **1979**, *57* (4), 433−443.
(9) Mintus, F.; Hamel, S.; Krumm, W. Wet Process Rotary Cement Kilns: Modeling and Simulation. *Clean Technol. Environ. Policy* **2006**, *8* (2), 112−122.
(10) Li, S. Q.; Ma, L. B.; Wan, W.; Yao, Q. A Mathematical Model of Heat Transfer in a Rotary Kiln Thermo-Reactor. *Chem. Eng. Technol.* **2005**, *28* (12), 1480−1489.
(11) Engin, T.; Ari, V. Energy Auditing and Recovery for Dry Type Cement Rotary Kiln Systems−−A Case Study. *Energy Convers. Manage.* **2005**, *46* (4), 551−562.
(12) Söğüt, Z.; Oktay, Z.; Karakoç, H. Mathematical Modeling of Heat Recovery from a Rotary Kiln. *Appl. Therm. Eng.* **2010**, *30* (8−9), 817−825.
(13) Atmaca, A.; Yumrutaş, R. Analysis of the Parameters Affecting Energy Consumption of a Rotary Kiln in Cement Industry. *Appl. Therm. Eng.* **2014**, *66* (1−2), 435−444.
(14) Utlu, Z.; Sogut, Z.; Hepbasli, A.; Oktay, Z. Energy and Exergy Analyses of a Raw Mill in a Cement Production. *Appl. Therm. Eng.* **2006**, *26* (17−18), 2479−2489.
(15) Nasution, M. H.; Syahputra, I. R.; Rahman, D. Energy and Exergy Analysis on the Rotary Kiln Unit of RKC-2 PT. Semen Gresik − Tuban Plant. *IOP Conf. Ser.: Mater. Sci. Eng.* **2021**, *1143* (1), No. 012050.
(16) Boateng, A. A. *Rotary Kilns: Transport Phenomena and Transport Processes*; Butterworth-Heinemann: Burlington, MA, 2006; pp 1−304.
(17) Ustaoglu, A.; Alptekin, M.; Akay, M. E. Thermal and Exergetic Approach to Wet Type Rotary Kiln Process and Evaluation of Waste Heat Powered ORC (Organic Rankine Cycle). *Appl. Therm. Eng.* **2017**, *112*, 281−295.
(18) Sahoo, N.; Kumar, A.; Samsher. Review on Energy Conservation and Emission Reduction Approaches for Cement Industry. *Environ. Dev.* **2022**, *44*, No. 100767.
(19) Acharya, P.; Fogo, D.; McBride, C. Process Challenges in Rotary Kiln-based Incinerators in Soil Remediation Projects. *Environ. Prog.* **1996**, *15* (4), 267−276.
(20) Shahin, H.; Hassanpour, S.; Saboonchi, A. Thermal Energy Analysis of a Lime Production Process: Rotary Kiln, Preheater and Cooler. *Energy Convers. Manage.* **2016**, *114*, 110−121.
(21) Gorog, J. P.; Adams, T. N.; Brimacombe, J. K. Regenerative Heat Transfer in Rotary Kilns. *Metall. Trans. B* **1982**, *13* (2), 153−163.
(22) Mujumdar, K. S.; Arora, A.; Ranade, V. V. Modeling of Rotary Cement Kilns: Applications to Reduction in Energy Consumption. *Ind. Eng. Chem. Res.* **2006**, *45* (7), 2315−2330.
(23) Mujumdar, K. S.; Ranade, V. V. Simulation of Rotary Cement Kilns Using a One-Dimensional Model. *Chem. Eng. Res. Des.* **2006**, *84* (3 A), 165−177.
(24) Eckert, E. R. G. Radiative Transfer, H. C. Hottel and A. F. Sarofim, McGraw-Hill Book Company, New York, 1967. 52 Pages. *AIChE J.* **1969**, *15* (5), 794−796.
(25) Howell, J. R.; Mengüç, M. P.; Daun, K. J.; Siegel, R. *Thermal Radiation Heat Transfer*, 7th ed.; CRC Press: Boca Raton, FL, 2021; pp 1−974.
(26) Modest, M. F. *Radiative Heat Transfer*; Elsevier, 2013.
(27) Gunnarsson, A.; Andersson, K.; Adams, B. R.; Fredriksson, C. Discrete-Ordinates Modelling of the Radiative Heat Transfer in a Pilot-Scale Rotary Kiln. *Energies* **2020**, *13* (9), No. 2192.
(28) Ehlmé, E.; Gunnarsson, A.; Andersson, K.; Normann, F. Heat Transfer Conditions in Hydrogen-Fired Rotary Kilns for Iron Ore Processing. *Ind. Eng. Chem. Res.* **2023**, *62* (37), 15098−15108.
(29) Gunnarsson, A.; Andersson, K.; Adams, B. R.; Fredriksson, C. Full-Scale 3D-Modelling of the Radiative Heat Transfer in Rotary Kilns with a Present Bed Material. *Int. J. Heat Mass Transfer* **2020**, *147*, No. 118924.
(30) Gunnarsson, A.; Bäckström, D.; Johansson, R.; Fredriksson, C.; Andersson, K. Radiative Heat Transfer Conditions in a Rotary Kiln Test Furnace Using Coal, Biomass, and Cofiring Burners. *Energy Fuels* **2017**, *31* (7), 7482−7492.
(31) Liu, X. Y.; Specht, E. Temperature Distribution within the Moving Bed of Rotary Kilns: Measurement and Analysis. *Chem. Eng. Process.: Process Intensif.* **2010**, *49* (2), 147−150.
(32) Jacob, R. M.; Tokheim, L.-A. Novel Design of a Rotary Calciner Internally Heated with Electrical Axial Heaters: Experiments and Modelling. *Results Eng.* **2023**, *17*, No. 100992.
(33) Boateng, A. A. Rotary Kiln Transport Phenomena: A Study of the Bed Motion and Heat Transfer. Ph.D. Thesis, University of British Columbia: Vancouver, Canada, 1993.
(34) Butler, B. W.; Denison, M. K.; Webb, B. W. Radiation Heat Transfer in a Laboratory-Scale, Pulverized Coal-Fired Reactor. *Exp. Therm. Fluid Sci.* **1994**, *9* (1), 69−79.
(35) Watkinson, A. P.; Brimacombe, J. K. Limestone Calcination in a Rotary Kiln. *Metall. Trans. B* **1982**, *13* (3), 369−378.
(36) Moumin, G.; Tescari, S.; Sattler, C. Impact of Bed Motion on the Wall-to-Bed Heat Transfer for Powders in a Rotary Kiln and Effect of Built-Ins. *Int. J. Heat Mass Transfer* **2021**, *177*, No. 121473.
(37) Gaurav, G. K.; Khanam, S. Analysis of Temperature Profile and % Metallization in Rotary Kiln of Sponge Iron Process through CFD. *J. Taiwan Inst. Chem. Eng.* **2016**, *63*, 473−481.
(38) Sass, A. Simulation of Heat Transfer Phenomena in a Rotary Kiln. *Ind. Eng. Chem. Process Des. Dev.* **1968**, *7* (2), 319−320.
(39) Spang, H. A. A Dynamic Model of a Cement Kiln. *Automatica* **1972**, *8* (3), 309−323.
(40) Guruz, H. K.; Bac, N. Mathematical Modelling of Rotary Cement Kilns by the Zone Method. *Can. J. Chem. Eng.* **1981**, *59* (4), 540−548.
(41) Singh, A. P.; Ghoshdastidar, P. S. Computer Simulation of Heat Transfer in Alumina and Cement Rotary Kilns. *J. Therm Sci. Eng. Appl.* **2022**, *14* (3), No. 031001, DOI: 10.1115/1.4051376.
(42) Bäckström, D.; Johansson, R.; Andersson, K.; Wiinikka, H.; Fredriksson, C. On the Use of Alternative Fuels in Rotary Kiln Burners — An Experimental and Modelling Study of the Effect on the Radiative Heat Transfer Conditions. *Fuel Process. Technol.* **2015**, *138*, 210−220.

(43) Andersson, K.; Johansson, R.; Johnsson, F.; Leckner, B. Radiation Intensity of Propane-Fired Oxy-Fuel Flames: Implications for Soot Formation. *Energy Fuels* **2008**, *22* (3), 1535−1541.
(44) Andersson, K.; Johansson, R.; Hjärtstam, S.; Johnsson, F.; Leckner, B. Radiation Intensity of Lignite-Fired Oxy-Fuel Flames. *Exp. Therm. Fluid Sci.* **2008**, *33* (1), 67−76.
(45) Barr, P. V.; Brimacombe, J. K.; Watkinson, A. P. A Heat-Transfer Model for the Rotary Kiln: Part II. Development of the Cross-Section Model. *Metall. Trans. B* **1989**, *20* (3), 403−419.
(46) Sullivan, J. D.; Maier, C. G.; Ralston, O. C. *Passage of Solid Particles through Rotary Cylindrical Kilns*; U.S. Bureau of Mines Technical, 1927.

https://doi.org/10.1021/acs.iecr.5c00704
Ind. Eng. Chem. Res. XXXX, XXX, XXX−XXX